Modeling Autoregulation of the Afferent Arteriole of the Rat Kidney

Veronica Ciocanel*, Tracy L. Stepien*, Aurélie Edwards, and Anita T. Layton

Abstract One of the key autoregulatory mechanisms that control blood flow in the kidney is the myogenic response. Subject to increased pressure, the renal afferent arteriole responds with an increase in muscle tone and a decrease in diameter. To investigate the myogenic response of an afferent arteriole segment of the rat kidney, we extend a mathematical model of an afferent arteriole cell. For each cell, we include detailed Ca^{2+} signaling, transmembrane transport of major ions, the kinetics of myosin light chain phosphorylation, as well as cellular contraction and wall mechanics. To model an afferent arteriole segment, a number of cell models are connected in series by gap junctions, which link the cytoplasm of neighboring cells. Blood flow through the afferent arteriole is modeled using Poiseuille flow. Simulation of an inflow pressure up-step leads to a decrease in the diameter for the proximal part of the vessel (vasoconstriction) and to an increase in proximal vessel diameter (vasodilation) for an inflow pressure down-step. Through its myogenic response, the afferent arteriole segment model yields approximately stable single-nephron glomerular filtration rate for a physiological range of inflow pressures (100–160

*The first and second authors made equal contributions.

Veronica Ciocanel
Division of Applied Mathematics, Brown University, Rhode Island, USA e-mail: veronica_ciocanel@brown.edu

Tracy L. Stepien
School of Mathematical and Statistical Sciences, Arizona State University, Tempe, Arizona, USA e-mail: tstepien@asu.edu

Aurélie Edwards
Sorbonne Universités, UPMC Univ Paris 06, Université Paris Descartes, Sorbonne Paris Cité, INSERM UMRS 1138, CNRS ERL 8228, Centre de Recherche des Cordeliers, Paris, France e-mail: aurelie.edwards@crc.jussieu.fr

Anita T. Layton
Department of Mathematics, Duke University, North Carolina, USA e-mail: alaytaon@math.duke.edu

mmHg), consistent with experimental observations. The present model can be incorporated as a key component into models of integrated renal hemodynamic regulation.

1 Introduction

In addition to waste excretion, the kidney is responsible for regulating the balance of water, electrolytes, and acid–base species. To accomplish these tasks, the kidney filters a portion of its blood supply into its functional units, the nephrons. Nephrons are elongated tubules surrounded by a layer of epithelial cells. As the filtrate flows through the nephron, its fluid and solutes are selectively reabsorbed or secreted, depending on the animal's physiological state. Consequently, the composition of the tubular fluid changes significantly along the nephron, until it eventually emerges as urine.

For the kidney to properly perform its functions, the rate of filtration into the nephron must be maintained within a narrow range. Thus, blood flow in the kidney is controlled by *autoregulatory mechanisms*. One of the key autoregulatory mechanisms is the tubuloglomerular feedback system, a negative feedback loop that seeks to balance the filtered load of sodium with the reabsorptive capacity of the nephron (Eaton and Pooler [4], Schnermann and Briggs [14]). That goal is accomplished by sensing alterations in tubular fluid chloride concentration at a certain location (alongside the macula densa cells) and then adjusting the muscle tension of the afferent arteriole, and thus renal blood flow and filtration rate, appropriately.

Another key autoregulatory mechanism is the myogenic response, which is an intrinsic property of the afferent arteriole. This mechanism induces a compensatory vasoconstriction of the afferent arteriole when the vessel is presented with an increase in transmural pressure.

The afferent arteriole thus plays a critical role in renal autoregulation. Edwards and Layton [5] previously developed a very detailed mathematical model of Ca^{2+} signaling within an afferent arteriole smooth muscle cell of the rat kidney. The model represents the transmembrane transport of major ions, intracellular Ca^{2+} dynamics, the kinetics of myosin light chain phosphorylation, and the mechanical behavior of the cell. The goal of the present study is to develop a multi-cell model of the afferent arteriole by connecting a series of afferent arteriole smooth muscle cells via gap junction coupling, and to use the model to study the myogenic response of the vessel. The present afferent arteriole model is intended to be employed as an essential component in models of integrated renal hemodynamic regulation.

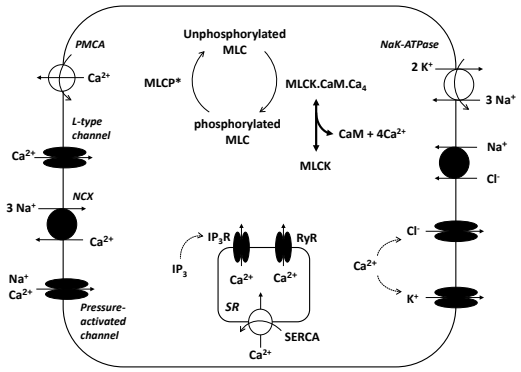

Fig. 1 Representation of a single afferent arteriole smooth muscle cell. The contractile force of the cell depends on the fraction of myosin light chains (MLC) that are phosphorylated. An increase of luminal pressure results in an influx of cations into the cytosol via pressure-activated channels. The ensuing depolarization leads to an increase in cytosolic Ca^{2+} levels, which then enhances the formation of the MLCK.CaM.Ca_4 complex (the active form of myosin light chain kinase, MLCK). Not shown in the diagram are the background currents and the inward- and delayed-rectifier K^+ channels. MLCP: myosin light chain phosphatase; CaM: calmodulin; PMCA: plasma membrane Ca^{2+} pump; NCX: Na^+/Ca^{2+} exchanger; SERCA: sarco/endoplasmic Ca^{2+} pump; RyR: ryanodine receptor; IP_3R: inositol triphosphate (IP_3) receptor.

2 Mathematical Model

In this section, we summarize the model of a single afferent arteriole smooth muscle cell of the rat kidney, previously developed by Edwards and Layton [5], and then extend this model to a segment of multiple smooth muscle cells that are connected in series via gap junctions.

2.1 Single Cell Model

The main signaling pathways in a single afferent arteriole smooth muscle cell that were considered in Edwards and Layton [5] are represented in Figure 1.

Considering the K^+, Na^+, Cl^-, and Ca^{2+} channels, the net sum of the currents flowing across the plasma membrane is

$$I_{\text{net}} = I_{\text{K,b}} + I_{\text{K,ir}} + I_{\text{K,v}} + I_{\text{K,Ca}} + I_{\text{NaK}} + I_{\text{Na,b}} + I_{\text{Na,Pres}} + I_{\text{NCX}} + I_{\text{Cl,b}} + I_{\text{Cl,Ca}} + I_{\text{Ca,b}} + I_{\text{Ca,Pres}} + I_{\text{PMCA}} + I_{\text{Ca,L}}, \quad (1)$$

and the transmembrane potential V_{m} is described by the differential equation

Table 1 Electrochemical parameters of the cell (overall)

Parameter	Value	Unit	Definition
C_{m}	5.5×10^{-6}	μF	Plasma membrane capacitance
$[\mathrm{K}]_{\mathrm{out}}$	5.4	mM	Extracellular K^+ concentration
$[\mathrm{Na}]_{\mathrm{out}}$	140	mM	Extracellular Na^+ concentration
$[\mathrm{Cl}]_{\mathrm{out}}$	120	mM	Extracellular Cl^- concentration
$[\mathrm{Ca}]_{\mathrm{out}}$	2	mM	Extracellular Ca^{2+} concentration
F	96,487	C/mol	Faraday constant
R	8.341	$\mathrm{J\cdot mol^{-1}\cdot K^{-1}}$	Ideal gas constant
T	298	K	Temperature
$\mathrm{vol}_{\mathrm{cyt}}$	1	pl	Volume of cytosol
$\mathrm{vol}_{\mathrm{cyt,Ca}}$	0.7	pl	Volume of cytosol accessible to Ca^{2+}
$\mathrm{vol}_{\mathrm{SR}}$	0.14	pl	Volume of sarcoplasmic reticulum
$G_{\mathrm{gap}}/C_{\mathrm{m}}$	950	$\mathrm{s^{-1}}$	Ratio of gap junction coefficient-to-membrane capacitance

$$\frac{dV_{\mathrm{m}}}{dt} = -\frac{I_{\mathrm{net}}}{C_{\mathrm{m}}}, \tag{2}$$

where C_{m} is the membrane capacitance. Parameter values and definitions are given in Table 1.

The *pressure-activated ion channels* are assumed to predominately carry Na^+ and be somewhat permeable to Ca^{2+} but not to other ions. The currents across these channels are

$$I_{\mathrm{Na,Pres}} = G_{\mathrm{Na,Pres}}(V_{\mathrm{m}} - E_{\mathrm{Na}}), \tag{3a}$$
$$I_{\mathrm{Ca,Pres}} = G_{\mathrm{Ca,Pres}}(V_{\mathrm{m}} - E_{\mathrm{Ca}}), \tag{3b}$$

where the conductances $G_{\mathrm{Na,Pres}}$ and $G_{\mathrm{Ca,Pres}}$ depend on the luminal pressure P as

$$G_{i,\mathrm{Pres}} = G^0_{i,\mathrm{Pres}}\left[1 + 1.75\left(\frac{P}{P_1} - 1\right)\left(1 + \frac{|P-P_2|}{P_2}\right)\right], \tag{4}$$

for $i = \mathrm{Na}^+, \mathrm{Ca}^{2+}$, with $P_1 = 100$ mmHg and $P_2 = 60$ mmHg.

The remaining equations describing transmembrane ionic transport (including ion and charge conservation equations, background currents, and K^+, Na^+, Cl^-, and Ca^{2+} transport pathways), intracellular Ca^{2+} dynamics (including Ca^{2+} buffers such as calmodulin), the kinetics of myosin light chain (MLC) phosphorylation, and vessel mechanics for the single cell model are described in the Appendix.

2.2 Multi-Cell Model

To extend the afferent arteriole smooth muscle single cell model of Edwards and Layton [5] to an afferent arteriole segment containing multiple smooth muscle cells,

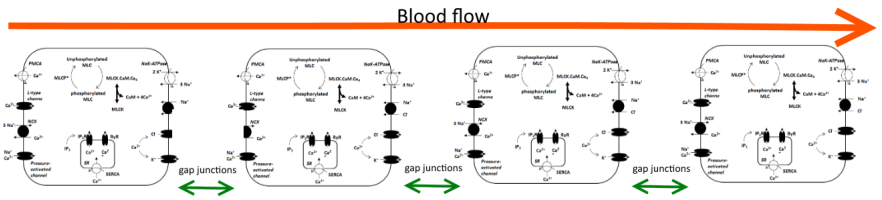

Fig. 2 Representation of a segment of multiple afferent arteriole smooth muscle cells in series. Each cell follows the dynamics of the single cell model (as in Figure 1), and the cells are connected to their immediate neighbors via gap junctions. Blood flow through the afferent arteriole lumen is described by Poiseuille flow (6).

we assume that each cell follows the dynamics of the single cell model as described in the previous section and the Appendix, and that all the cells are connected in series via gap junctions. Gap junctions directly connect the cytoplasm of neighboring cells and allow ions to pass through them, thus coupling the cells electrically. The flow of ions carrying an electric charge causes an almost instantaneous diffusion of electrical disturbance to a neighboring cell.

Hence, we modify equation (2) for the transmembrane potential of a single cell to a segment of cells (see Figure 2) where the electric charge of a given cell j may diffuse between its nearest neighbors $j+1$ and $j-1$ such that

$$\frac{dV_{\mathrm{m}}^{j}}{dt} = -\frac{I_{\mathrm{net}}}{C_{\mathrm{m}}} - \frac{G_{\mathrm{gap}}}{C_{\mathrm{m}}}\left(-V_{\mathrm{m}}^{j+1} + 2V_{\mathrm{m}}^{j} - V_{\mathrm{m}}^{j-1}\right), \qquad j = 2,\ldots,N_{\mathrm{cell}}-1, \tag{5a}$$

$$\frac{dV_{\mathrm{m}}^{j}}{dt} = 0, \qquad j = 1, N_{\mathrm{cell}}, \tag{5b}$$

where N_{cell} is the total number of cells and G_{gap} is the gap junction coefficient, which denotes the strength of the coupling; we assume that $G_{\mathrm{gap}}/C_{\mathrm{m}} = 950\ \mathrm{s}^{-1}$ (Sgouralis and Layton [15]). Per our convention, $j = 1$ is the first upstream cell and $j = N_{\mathrm{cell}}$ is the last downstream cell.

As blood flows through the segment of smooth muscle cells, the inflow and outflow pressures vary from cell to cell. The luminal blood flow is assumed to be at a quasi-steady state and is therefore described by Poiseuille flow

$$\frac{dP}{dx} = -\frac{8\mu Q}{\pi R^4}, \tag{6}$$

where P is the hydrostatic pressure, μ is the dynamic viscosity of blood, Q is the volumetric flow rate, and R is the luminal radius calculated from the diameter equation (43).

Once the radius R is determined, the hydrostatic pressure P for each cell is updated. This, in turn, affects the pressure-activated ion channel conductances $G_{\mathrm{Na,Pres}}$ and $G_{\mathrm{Ca,Pres}}$ (equation (4)), which are modified as

$$G_{i,\mathrm{Pres}} = \max\left\{0, \quad 20 + 0.35(P - \bar{P}_0)\left(1 + \frac{\max\{0,\, P - P_1\}}{P_1}\right)\right\}, \tag{7}$$

for $i = \mathrm{Na}^+, \mathrm{Ca}^{2+}$. In the above equation, the conductance is expressed in pS, $P_1 =$ 60 mmHg, and $\bar{P}_0$ is a reference pressure that decreases approximately linearly from 100 mmHg to 91.45 mmHg along the model afferent arteriole.

2.3 Numerical Method

To numerically solve the multi-cell model, we implement fractional splitting: the single cell model is solved for each cell separately in the first stage, and the diffusion of electric charge between all cells is taken into account in the second stage.

Letting $\mathscr{R}$ represent the nonlinear reaction part of equation (5a) (the first term) and f_j^i be the solution to the 51 ordinary differential equations (solved with ode15s in MATLAB) of the single cell model for cell $j = 1, \ldots, N_{\mathrm{cell}}$ at time step i with $\mathbf{f}^i = (f_1^i, f_2^i, \ldots, f_{N_{\mathrm{cell}}}^i)$, the first step in the splitting is

$$\frac{\mathbf{f}^* - \mathbf{f}^i}{\Delta t} = \mathscr{R}(\mathbf{f}^*), \tag{8}$$

where $\mathbf{f}^* = (f_1^*, f_2^*, \ldots, f_{N_{\mathrm{cell}}}^*)$ is the predicted solution that will be corrected by the second step.

Let $\hat{f}_j^*$ be the portion of the solution f_j^* that represents the transmembrane potential V_{m} for cell j with $\hat{\mathbf{f}}^* = (\hat{f}_1^*, \hat{f}_2^*, \ldots, \hat{f}_{N_{\mathrm{cell}}}^*)$. The linear diffusion part of equation (5a) (the second term) is solved with ode45 with Neumann boundary conditions (5b) in MATLAB and is

$$\frac{\hat{\mathbf{f}}^{i+1} - \hat{\mathbf{f}}^*}{\Delta t} = \frac{G_{\mathrm{gap}}}{C_{\mathrm{m}}} \Delta \hat{\mathbf{f}}^{i+1}, \tag{9}$$

where $\hat{\mathbf{f}}^{i+1}$ replaces the transmembrane potential portion of $\mathbf{f}^*$ to obtain $\mathbf{f}^{i+1}$, the solution at time step $i+1$.

Assuming that the inflow pressure applied to the first cell, P_1, is constant throughout time, the hydrostatic pressure for the other cells, P_j, $j = 2, \ldots, N_{\mathrm{cell}}$, is then updated from the Poiseuille flow (6), which is discretized such that

$$P_{j+1}^{i+1} = P_j^{i+1} - \frac{8\mu Q}{\pi (R_{j+1})^4} \Delta x, \qquad j = 2, \ldots, N_{\mathrm{cell}}, \tag{10}$$

where Δx is the numerical width of one afferent arteriole smooth muscle cell subsegment.

In the case where the inflow pressure is varied linearly between some times $\hat{t}_1$ and $\hat{t}_2$, then P_1 is discretized as

$$P_1^{i+1} = P_1^i - \hat{p} \frac{\Delta t}{\hat{t}_2 - \hat{t}_1}, \tag{11}$$

Table 2 Parameters for Poiseuille equation for blood flow through the afferent arteriole

Parameter	Value	Unit	Definition
μ	1.26×10^{-4}	mmHg · s	Dynamic viscosity of blood
Q	300	nL/min	Volumetric flow rate

where $\hat{p}$ determines the change in perfusion pressure that is applied to the first cell from time $\hat{t}_1$ to $\hat{t}_2$.

3 Model Results

We apply our blood vessel model to an afferent arteriole of length ~ 240 μm. The parameters we use for the single cell model are given in Table 1 and the tables in the Appendix. Additionally, the Poiseuille equation (6) parameters are given in Table 2, where we assume that the volumetric flow rate Q is known *a priori*. The model afferent arteriole is discretized into $N_{\text{cell}} = 20$ numerical cells, each of length $\Delta x = 12$ μm.

The base case corresponds to setting the inflow boundary pressure to 100 mmHg. Figure 3 shows the oscillations in membrane potential V_{m} predicted by the model for the first cell in our afferent arteriole segment. The mean value of the transmembrane potential is -36 mV, which is a good approximation of the measured value of -40 mV in the pressurized afferent arteriole. The cytosolic concentration of Ca^{2+} in this cell is shown in Figure 4. This concentration oscillates between 220 and 320 nM, similar to the range predicted by the single-cell model in Edwards and Layton [5]. Similar oscillations are predicted for the other cells (results not shown).

The diameter of the vessel at the location of the first cell also shows an oscillatory time profile, which slowly stabilizes to an average of 20.1 μm, as can be seen in

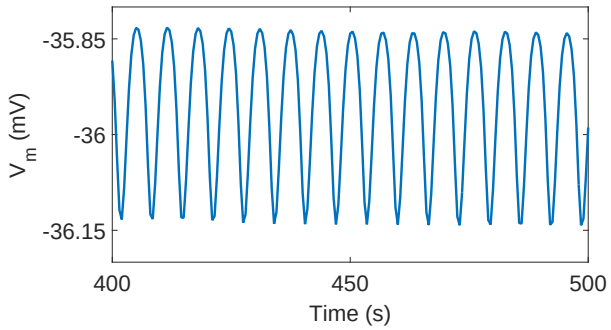

Fig. 3 Predicted oscillations of the membrane potential V_{m} for the first cell in the afferent arteriole at an inflow pressure of 100 mmHg.

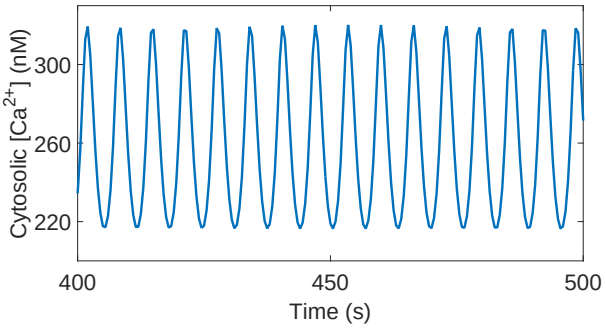

Fig. 4 Predicted oscillations of the cytosolic concentration of Ca^{2+} for the first cell in the afferent arteriole at an inflow pressure of 100 mmHg.

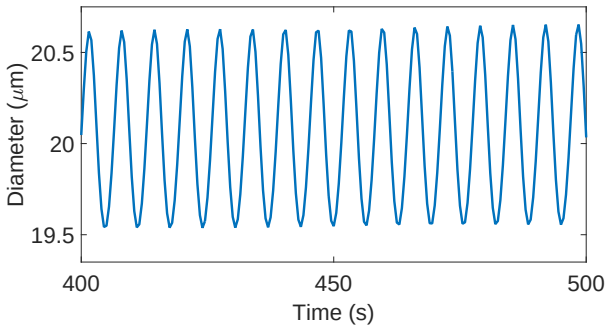

Fig. 5 Predicted oscillations of the afferent arteriole diameter at the first cell coordinate at an inflow pressure of 100 mmHg.

Figure 5. We note that this value is only slightly smaller than the average luminal diameter of 20.5 μm predicted by the single cell model in Edwards and Layton [5].

We examined the effects of varying the inflow pressure on the afferent arteriole. The left panels in Figure 6 correspond to model simulations where the inflow pressure starts at the reference value of 100 mmHg, then from 50 to 150 seconds we increase this pressure linearly to 120 mmHg, and then keep it constant at this higher level for the remainder of the simulation. In a separate simulation, we follow a similar protocol and decrease the luminal pressure linearly to 90 mmHg and then keep it constant at this lower level to produce the panels on the right.

In the case of a pressure increase, we note that this change opens the pressure-activated channels and triggers depolarization, thereby raising the transmembrane potential V_m and, subsequently, the cytosolic concentration of Ca^{2+}. In the pressure down-step case, we observe a reduction in V_m, which elicits a decrease in cytosolic $[Ca^{2+}]$ and leads to an oscillatory regime for this concentration. These observations are similar to single-cell model results in Edwards and Layton [5], where luminal pressure was sharply increased or reduced at a given time point.

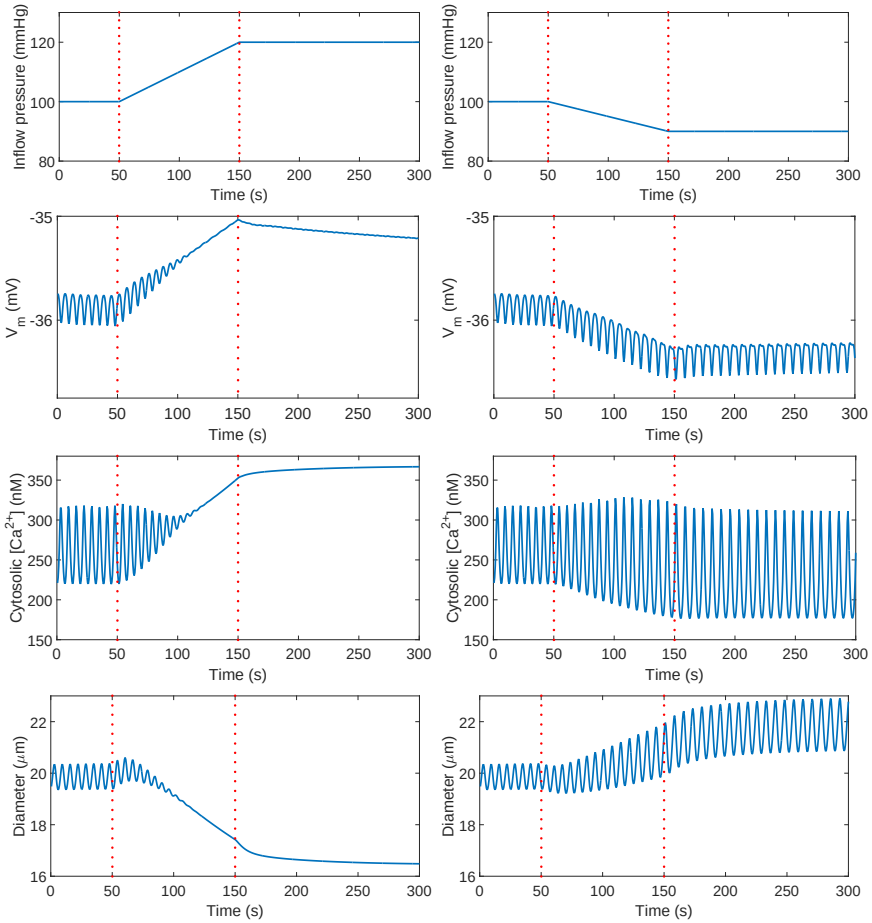

Fig. 6 Time profiles of inflow pressure, V_{m}, cytosolic [Ca^{2+}], and vessel diameter with a pressure increase to 120 mmHg (left) and a pressure decrease to 90 mmHg (right). The red dotted vertical lines point to the time interval when luminal pressure is linearly increased (left) or decreased (right).

The last row of Figure 6 shows that the diameter of the vessel at the coordinate of the first cell oscillates around 20 μm before $t = 50$ s, as in Figure 5. At $t = 50$ s, the arteriole acts as a compliant tube and dilates as pressure increases, and conversely constricts as pressure decreases. This passive response was also observed in the single-cell model of Edwards and Layton [5].

This effect is quickly replaced by the myogenic response, which leads to a decrease in the vessel diameter (vasoconstriction) for the pressure up-step and an increase in diameter (vasodilation) for the pressure down-step. The vessel diameter stabilizes around 16 μm for the pressure up-step, and stably oscillates around 22 μm for the pressure down-step. The plots correspond to the first cell in the vessel

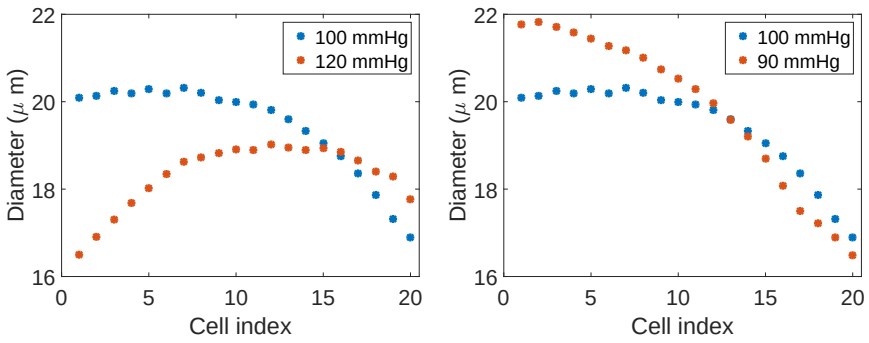

Fig. 7 Time-averaged luminal diameters along the blood vessel for base case inflow pressure 100 mmHg together with pressure increase to 120 mmHg (left) and pressure decrease to 90 mmHg (right).

for both simulations, and a similar myogenic response controls the time profile of diameters of all subsequent cells (results not shown).

The effects of base case pressure, pressure up-step and down-step on all vessel cells are shown in Figure 7. Each blue dot corresponds to the average diameter at a given cell location over a time interval where the radius stabilizes (either converges to a specific value or oscillates around it). The base case pressure of 100 mmHg shows relatively constant diameters for the first (proximal) part of the vessel, and a decrease to 16.9 μm in the distal (latter) part of the segment. For the increase in luminal pressure to 120 mmHg, our model predicts vasoconstriction in the proximal part of the afferent arteriole segment, which is reflected in the left panel of Figure 7 by the low diameters at the level of the first cells. The myogenic response stabilizes downstream pressure, thereby raising the radius in the distal part of the afferent arteriole segment to 17.8 μm despite the pressure up-step. Conversely, a pressure down-step elicits the expected vasodilation in the proximal afferent arteriole segment, as shown in the right panel; its myogenic response yields a distal afferent arteriole diameter that is smaller than the proximal afferent arteriole diameter (16.5 μm at the end cell).

It is worth noting that the diameters in the distal part of the afferent arteriole segment drop back to lower values in the case of the inflow pressure up-step (see left panel of Figure 7). In order to understand this effect, we should note that the afferent arteriole diameter represents a balance between the elastic force of the cell and the myogenic response (see equation (43)). As we move along the afferent arteriole, the luminal pressure decreases, so that the myogenic response is dominant and leads to the increase in diameter for the pressure up-step case. Towards the end of the vessel, the pressure becomes much lower and thus the elastic force (which is proportional to pressure) leads to a decrease in the distal afferent arteriole diameter.

In order to further investigate the model afferent arteriole's myogenic response, we computed the outflow pressure and time- and space-averaged diameter of the afferent arteriole given different constant inflow pressures. Figure 8 shows the pre-

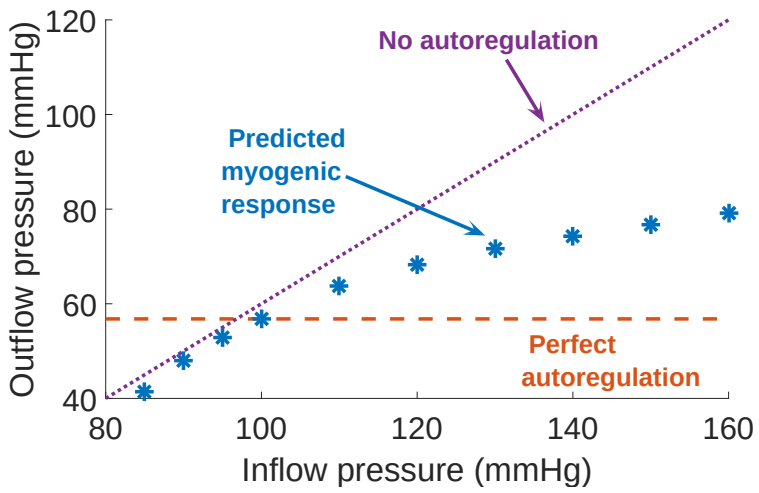

Fig. 8 Predicted myogenic response (blue) compared to perfect autoregulation (purple) and no autoregulation (orange) of blood flow through the vessel for a range of luminal pressures.

dicted outflow pressures at the level of the last afferent arteriole cell. Our results suggest that there is a slow increase in the outflow pressure for reference inflow pressures between 100 and 160 mmHg. This increase is substantially slower than a slope 1 line that would represent no autoregulation, and highlights the predicted myogenic response of the afferent arteriole model. Note that the predicted outflow pressure of about 80 mmHg for an inflow pressure of 160 mmHg is higher than the 50 mmHg outflow pressure predicted in Sgouralis and Layton [15].

Similarly, Figure 9 shows the space- and time-averaged afferent arteriole diameter for different reference pressure inputs. As in Sgouralis and Layton [15], the results point to vasodilation for small inflow pressures (85 mmHg) where the mean diameter is around 20 μm, and vasoconstriction for large inflow pressures (160 mmHg), where the mean diameter is lower, around 16.5 μm.

4 Discussion

We have developed a mathematical model of a segment of the afferent arteriole of the rat kidney. The model represents detailed Ca^{2+} trafficking in each of the afferent arteriole smooth muscle cells, as well as the kinetics of myosin light chain phosphorylation and the mechanical behavior of the cell. The multi-cell afferent arteriole model is an extension of our published cell model [5], which represents the Ca^{2+} dynamics and vasoresponse of a single afferent arteriole smooth muscle cell. The afferent arteriole segment model of the present study was constructed by connecting 20 afferent arteriole cell models in series; each cell model is coupled

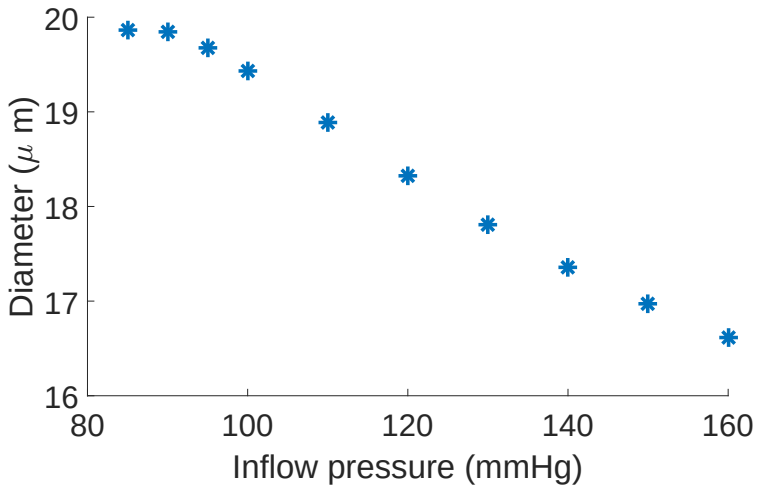

Fig. 9 Predicted space- and time-averaged afferent arteriole diameter for a range of luminal pressures.

to its neighbors through gap junctions, which allow the representation of electric conduction along the afferent arteriole. A fluid dynamics model was included to relate fluid pressure, fluid flow, and tubular resistance.

The model predicts spontaneous vasomotion at physiological luminal pressures, which arises from the dynamic exchange of Ca^{2+} between the cytosol and the sarcoplasmic reticulum, coupled to the stimulation of Ca^{2+}-activated potassium (K_{Ca}) and chloride (Cl_{Ca}) channels, and the modulation of voltage-activated L-type channels. These spontaneous oscillations of the afferent arteriole muscle tone result in oscillations in fluid pressure and flow.

It is well known that the renal afferent arteriole exhibits the *myogenic response*, wherein it reacts to an elevation in blood pressure with an increase in muscle tone and a decrease in luminal diameter. The myogenic response is believed to stabilize glomerular filtration and to protect the glomerulus from exceedingly high systolic blood pressure, especially in hypertension. The model represents the myogenic response by assuming that the response is initiated by pressure-induced changes in the activity of non-selective cation channels. Through its myogenic response, the model afferent arteriole stabilizes, to a significant degree, outflow pressure for a range of steady-state inflow pressure, from 100–160 mmHg (see Figure 8).

With its representation of the myogenic response, the present afferent arteriole segment model can be used as an essential component in models of integrated renal hemodynamic regulation. By coupling a number of afferent arteriole segment models, one can investigate how vasomotor responses propagate among a vascular tree. Furthermore, as we have previously done using a simpler model of an afferent arteriole segment (Sgouralis and Layton [16]), the present model could be combined with a model of glomerular filtration (e.g., Deen et al. [3], Sgouralis and Layton [16]) and a model of the tubuloglomerular feedback mechanism (e.g., Layton [12], Sgouralis

and Layton [16]), which is another key renal autoregulatory mechanism. The resulting integrative model of renal hemodynamics could then serve to investigate the interactions between the myogenic and TGF mechanisms in the context of renal autoregulation.

5 Appendix

This appendix contains the remaining equations besides the ones given in Section 2.1 for the afferent arteriole smooth muscle single cell model of Edwards and Layton [5]. For further details and kinetic diagrams, refer to [5].

5.1 Transmembrane Ionic Transport

5.1.1 Ion and charge conservation equations

The cytosolic concentrations of K^+, Na^+, Cl^-, and Ca^{2+} are determined by considering the net sum of their respective fluxes into the cytosol (described in subsequent sections) and integrating

$$\frac{d[\mathrm{K}]_{\mathrm{cyt}}}{dt} = -\frac{(I_{\mathrm{K,b}} + I_{\mathrm{K,ir}} + I_{\mathrm{K,v}} + I_{\mathrm{K,Ca}} - 2I_{\mathrm{NaK}})}{F \cdot \mathrm{vol}_{\mathrm{cyt}}}, \tag{12a}$$

$$\frac{d[\mathrm{Na}]_{\mathrm{cyt}}}{dt} = -\frac{(I_{\mathrm{Na,b}} + I_{\mathrm{Na,Pres}} + 3I_{\mathrm{NaK}} + 3I_{\mathrm{NCX}})}{F \cdot \mathrm{vol}_{\mathrm{cyt}}} + \frac{J_{\mathrm{NaCl}}}{\mathrm{vol}_{\mathrm{cyt}}}, \tag{12b}$$

$$\frac{d[\mathrm{Cl}]_{\mathrm{cyt}}}{dt} = \frac{I_{\mathrm{Cl,b}} + I_{\mathrm{Cl,Ca}}}{F \cdot \mathrm{vol}_{\mathrm{cyt}}} + \frac{J_{\mathrm{NaCl}}}{\mathrm{vol}_{\mathrm{cyt}}}, \tag{12c}$$

$$\frac{d[\mathrm{Ca}]_{\mathrm{cyt}}}{dt} = -\frac{\left(I_{\mathrm{Ca,b}} + I_{\mathrm{Ca,Pres}} + I_{\mathrm{PMCA}} + I_{\mathrm{Ca,L}} - 2I_{\mathrm{NCX}} + I_{\mathrm{SERCA}} - I_{\mathrm{RyR}} - I_{\mathrm{IP3R}}\right)}{2F \cdot \mathrm{vol}_{\mathrm{cyt,Ca}}} + R^{\mathrm{cyt}}_{\mathrm{CaM}} + R^{\mathrm{cyt}}_{\mathrm{Bf}}, . \tag{12d}$$

Parameter values and definitions are given in Table 1.

In the sarcoplasmic reticulum (SR),

$$\frac{d[\mathrm{Ca}]_{\mathrm{SR}}}{dt} = \frac{I_{\mathrm{SERCA}} - I_{\mathrm{RyR}} - I_{\mathrm{IP3R}}}{2F \cdot \mathrm{vol}_{\mathrm{SR}}} + R^{\mathrm{SR}}_{\mathrm{Calseq}}. \tag{13}$$

The reaction terms $R^{\mathrm{cyt}}_{\mathrm{CaM}}$, $R^{\mathrm{cyt}}_{\mathrm{Bf}}$, and $R^{\mathrm{SR}}_{\mathrm{Calseq}}$ account for the buffering of Ca^{2+} by cadmolin, other cytosolic buffers, and calsequestrin, respectively, and are described in equation (35) below.

5.1.2 Background currents

The background current of ion i, for $i = \mathrm{K}^+, \mathrm{Na}^+, \mathrm{Cl}^-, \mathrm{Ca}^{2+}$, is

$$I_{i,\mathrm{b}} = G_{i,\mathrm{b}} \left(V_\mathrm{m} - E_i \right), \tag{14}$$

where the Nernst potential of ion i with valence z_i is

$$E_i = \frac{RT}{z_i F} \ln \left(\frac{[i]_\mathrm{out}}{[i]_\mathrm{cyt}} \right). \tag{15}$$

Parameter values and definitions are given in Table 1.

5.1.3 Potassium transport pathways

The potassium current across inward-rectifier (K_ir) channels is determined as

$$I_{\mathrm{K,ir}} = G_\mathrm{Kir} P_\mathrm{Kir} \left(\frac{[K]_\mathrm{out}}{[K]_\mathrm{ref}} \right)^{0.9} \left(V_\mathrm{m} - E_\mathrm{K} \right), \tag{16a}$$

$$P_\mathrm{Kir} = \frac{1}{1 + \exp\left(\dfrac{V_\mathrm{m} - V_\mathrm{Kir}}{s_\mathrm{Kir}} \right)}, \tag{16b}$$

where the exponential factor, 0.9, the potential of half-maximal activation, V_Kir, and the slope, s_Kir, were obtained by fitting K_ir currents in cerebral arterial smooth muscle cells (Wu et al. [18]). Parameter values are given in Tables 1 and 3.

The potassium current across delayed-rectifier (K_v) channels is given by

Table 3 Parameters for potassium currents

Parameter	Value	Unit
$G_\mathrm{K,b}$	0	nS
G_Kir	0.50	nS
$[\mathrm{K}]_\mathrm{ref}$	5.0	mM
V_Kir	$-80/-65$	mV*
s_Kir	20/5	mV*
G_Kv	9.83	nS
G_KCa	5.0	nS
τ_Pf	0.5	mS
τ_Ps	11.5	mS

*Values for V_m below/above -60 mV

$$I_{\mathrm{K,v}} = G_{\mathrm{Kv}} \left(P_{\mathrm{Kv}}\right)^2 \left(V_{\mathrm{m}} - E_{\mathrm{K}}\right), \tag{17a}$$

$$P_{\mathrm{Kv}} = 0.58 P_{\mathrm{Kv1}} + 0.42 P_{\mathrm{Kv2}}, \tag{17b}$$

$$\frac{dP_{\mathrm{Kv1}}}{dt} = \frac{\bar{P}_{\mathrm{Kv}} - P_{\mathrm{Kv1}}}{\tau_{\mathrm{Kv1}}}, \tag{17c}$$

$$\frac{dP_{\mathrm{Kv2}}}{dt} = \frac{\bar{P}_{\mathrm{Kv}} - P_{\mathrm{Kv2}}}{\tau_{\mathrm{Kv2}}}, \tag{17d}$$

$$\bar{P}_{\mathrm{Kv}} = \frac{1}{1 + \exp\left(-\dfrac{V_{\mathrm{m}} + 1.77}{14.52}\right)}, \tag{17e}$$

$$\tau_{\mathrm{kv1}} = 210.99 \exp\left[-\left(\frac{V_{\mathrm{m}} + 214.34}{195.35}\right)^2\right] - 20.59, \tag{17f}$$

$$\tau_{\mathrm{kv2}} = 821.39 \exp\left[-\left(\frac{V_{\mathrm{m}} + 31.59}{27.46}\right)^2\right] + 0.189, \tag{17g}$$

where P_{Kv1} and P_{Kv2} are the two components of the channel activation process and τ_{Kv1} and τ_{Kv2} are the respective time constants (in ms) (Yang et al. [19]). Variable $\bar{P}_{\mathrm{Kv}}$ is voltage dependent and represents the steady-state value of P_{Kv1} and P_{Kv2}.

The potassium current across Ca^{2+}-activated K^+ (K_{Ca}) channels is computed as

$$I_{\mathrm{K,Ca}} = G_{\mathrm{KCa}} P_{\mathrm{KCa}} \left(V_{\mathrm{m}} - E_{\mathrm{K}}\right), \tag{18a}$$

$$P_{\mathrm{KCa}} = 0.65 P_{\mathrm{f}} + 0.35 P_{\mathrm{s}}, \tag{18b}$$

$$\frac{dP_{\mathrm{f}}}{dt} = \frac{\bar{P}_{\mathrm{KCa}} - P_{\mathrm{f}}}{\tau_{\mathrm{Pf}}}, \tag{18c}$$

$$\frac{dP_{\mathrm{s}}}{dt} = \frac{\bar{P}_{\mathrm{KCa}} - P_{\mathrm{s}}}{\tau_{\mathrm{Ps}}}, \tag{18d}$$

$$\bar{P}_{\mathrm{KCa}} = \frac{1}{1 + \exp\left(-\dfrac{V_{\mathrm{m}} - V_{\mathrm{KCa}}}{21.70}\right)}, \tag{18e}$$

$$V_{\mathrm{KCa}} = -45.0 \ \log_{10}\left([\mathrm{Ca}]_{\mathrm{cyt}}\right) - 63.55, \tag{18f}$$

where P_{f} and P_{s} are the fast and slow components of the channel activation process, respectively, and τ_{Pf} and τ_{Ps} are the corresponding time constants (Yang et al. [19]). The steady-state open probability of the channels is given by $\bar{P}_{\mathrm{KCa}}$.

The ATP-dependent K^+ channels are not considered in the Edwards and Layton model [5] since it assumed that their conductance is negligible in well perfused and oxygenated arterioles.

5.1.4 Sodium transport pathways

The current across Na^+/K^+-ATPase pumps is determined as

$$I_{\mathrm{NaK}} = I_{\mathrm{NaK,max}} \left(\frac{[K]_{\mathrm{out}}}{[K]_{\mathrm{out}} + K^{\mathrm{K}}_{\mathrm{m,NaK}}} \right)^2 \left(\frac{[\mathrm{Na}]_{\mathrm{cyt}}}{[\mathrm{Na}]_{\mathrm{cyt}} + K^{\mathrm{Na}}_{\mathrm{m,NaK}}} \right)^3 . \tag{19}$$

The current across Na^+/Ca^{2+} (NCX) exchanges is given by

$$I_{\mathrm{NCX}} = I_{\mathrm{NCX,max}} A_{\mathrm{NCX}} \left(\frac{\Phi_{\mathrm{F}}[\mathrm{Na}]^3_{\mathrm{cyt}}[\mathrm{Ca}]_{\mathrm{out}} - \Phi_{\mathrm{R}}[\mathrm{Na}]^3_{\mathrm{out}}[\mathrm{Ca}]_{\mathrm{cyt}}}{G(1 + k_{\mathrm{sat}}\Phi_{\mathrm{R}})} \right), \tag{20a}$$

$$A_{\mathrm{NCX}} = \frac{[\mathrm{Ca}]^2_{\mathrm{cyt}}}{\left(K^{\mathrm{Ca}}_{\mathrm{m,NCX}}\right)^2 + [\mathrm{Ca}]^2_{\mathrm{cyt}}}, \tag{20b}$$

$$\Phi_{\mathrm{F}} = \exp\left(\frac{\gamma V_{\mathrm{m}} F}{RT}\right), \tag{20c}$$

$$\Phi_{\mathrm{R}} = \exp\left(\frac{(\gamma - 1) V_{\mathrm{m}} F}{RT}\right), \tag{20d}$$

$$\begin{aligned} G = {} & [\mathrm{Na}]^3_{\mathrm{out}}[\mathrm{Ca}]_{\mathrm{cyt}} + [\mathrm{Na}]^3_{\mathrm{cyt}}[\mathrm{Ca}]_{\mathrm{out}} + K^3_{\mathrm{mNao}}[\mathrm{Ca}]_{\mathrm{cyt}} \\ & + K_{\mathrm{mCao}}[\mathrm{Na}]^3_{\mathrm{cyt}} + K^3_{\mathrm{mNai}}[\mathrm{Ca}]_{\mathrm{out}}\left(1 + [\mathrm{Ca}]_{\mathrm{cyt}}/K_{\mathrm{mCai}}\right) \\ & + K_{\mathrm{mCai}}[\mathrm{Na}]^3_{\mathrm{out}}\left(1 + [\mathrm{Na}]^3_{\mathrm{cyt}}/K^3_{\mathrm{mNai}}\right) \end{aligned} \tag{20e}$$

(Shannon et al [17]). The flux across NaCl cotransporters is computed as

$$J_{\mathrm{NaCl}} = J_{\mathrm{NaCl,max}} \frac{(E_{\mathrm{Na}} - E_{\mathrm{Cl}})^4}{(E_{\mathrm{Na}} - E_{\mathrm{Cl}})^4 + R^4_{\mathrm{NaCl}}} \tag{21}$$

(Kneller et al. [11]). Parameter values are given in Tables 1 and 4.

Table 4 Parameters for sodium currents

Parameter	Value	Unit
$G_{\mathrm{Na,b}}$	0.007	nS
$G^0_{\mathrm{Na,Pres}}$	0.020	nS
$I_{\mathrm{NaK,max}}$	3.75	μA/μF
$K^{\mathrm{K}}_{\mathrm{m,NaK}}$	1.5	mM
$K^{\mathrm{Na}}_{\mathrm{m,NaK}}$	12	mM
$I_{\mathrm{NCX,max}}$	1.5	μA/μF
$K^{\mathrm{Ca}}_{\mathrm{m,NCX}}$	0.125×10^{-3}	mM
k_{sat}	0.27	dimensionless

Parameter	Value	Unit
$K_{\mathrm{m,Nao}}$	87.5	mM
$K_{\mathrm{m,Cao}}$	1.3	mM
$K_{\mathrm{m,Nai}}$	12.29	mM
$K_{\mathrm{m,Cai}}$	3.59×10^{-3}	mM
γ	0.35	dimensionless
$J_{\mathrm{NaCl,max}}$	1.08×10^{-16}	mM/s
R_{NaCl}	87.825	mV

5.1.5 Chloride transport pathways

The current across Ca^{2+}-activated Cl^- (Cl_{Ca}) channels is

$$I_{\mathrm{Cl,Ca}} = G_{\mathrm{ClCa}} P_{\mathrm{ClCa}} (V_{\mathrm{m}} - E_{\mathrm{Cl}}), \tag{22a}$$

$$\frac{dP_{\mathrm{ClCa}}}{dt} = \frac{\bar{P}_{\mathrm{ClCa}} - P_{\mathrm{ClCa}}}{\tau_{\mathrm{ClCa}}}, \tag{22b}$$

$$\bar{P}_{\mathrm{ClCa}} = \frac{[\mathrm{Ca}]^3_{\mathrm{cyt}}}{[\mathrm{Ca}]^3_{\mathrm{cyt}} + K^3_{\mathrm{ClCa}}}, \tag{22c}$$

where $\bar{P}_{\mathrm{ClCa}}$ is the steady-state open probability of the channel (Jacobson et al. [8]). Parameter values are given in Table 5.

Table 5 Parameters for chloride currents

Parameter	Value	Unit
$G_{\mathrm{Cl,b}}$	0.007	nS
G_{ClCa}	0.80	nS
τ_{ClCa}	0.050	s
K_{ClCa}	140	mM

5.1.6 Calcium transport pathways

Calcium is exchanged between the cytosol and the extracellular space, and between the cytosol and the SR, which acts as a storage compartment. Parameter values for calcium currents and buffer reactions are given in Tables 1 and 6.

The current through plasmalemmal Ca^{2+} (PMCA) pumps is determined as

Table 6 Parameters for calcium currents and buffers

Parameter	Value	Unit	Parameter	Value	Unit
$G_{\mathrm{Ca,b}}$	0.007	nS	k_4	1.1×10^{-3}	mM
$G^0_{\mathrm{Ca,Pres}}$	0.003	nS	k^{IP3}_-	1.0	s^{-1}
G_{CaL}	2.75	nS	a_1	400×10^3	$\mathrm{mM}^{-1} \cdot \mathrm{s}^{-1}$
$I_{\mathrm{PMCA,max}}$	0.9	μA/μF	a_3	400×10^3	$\mathrm{mM}^{-1} \cdot \mathrm{s}^{-1}$
$K^{\mathrm{Ca}}_{\mathrm{m,PMCA}}$	170×10^{-6}	mM	a_4	0.2×10^3	$\mathrm{mM}^{-1} \cdot \mathrm{s}^{-1}$
$I_{\mathrm{SERCA,max}}$	11.76	pA	a_5	20×10^3	$\mathrm{mM}^{-1} \cdot \mathrm{s}^{-1}$
$K^{\mathrm{Ca}}_{\mathrm{m,SERCA}}$	310×10^{-6}	mM	d_1	0.13×10^{-3}	mM^{-1}
ν_{RyR}	12	s^{-1}	d_3	943.4×10^{-6}	mM^{-1}
K_{a}	3.7222×10^{-6}	mM	d_4	144.5×10^{-6}	mM^{-1}
K_{b}	6.3601×10^{-6}	mM	d_5	82.34×10^{-6}	mM^{-1}
K_{c}	0.0571	dimensionless	$K^{\mathrm{Bf}}_{\mathrm{on}}$	10^3	$\mathrm{mM}^{-1} \cdot \mathrm{s}^{-1}$
k^-_{c}	0.1	s^{-1}	$K^{\mathrm{Bf}}_{\mathrm{off}}$	5	s^{-1}
ν_{IP3R}	12	s^{-1}	$[\mathrm{Bf}]^{\mathrm{tot}}_{\mathrm{cyt}}$	0.50	mM
K^{IP3}_+	1.85	s^{-1}	$k^{\mathrm{Calseq}}_{\mathrm{on}}$	10^5	$\mathrm{mM}^{-1} \cdot \mathrm{s}^{-1}$
$[\mathrm{IP}_3]_{\mathrm{ref}}$	240	mM	$k^{\mathrm{Calseq}}_{\mathrm{off}}$	65	s^{-1}
α_4	0.5	dimensionless	$[\mathrm{Calseq}]^{\mathrm{tot}}_{\mathrm{SR}}$	0.14	mM

$$I_{\mathrm{PMCA}} = I_{\mathrm{PMCA,max}} \left(\frac{[\mathrm{Ca}]_{\mathrm{cyt}}}{K^{\mathrm{Ca}}_{\mathrm{m,PMCA}} + [\mathrm{Ca}]_{\mathrm{cyt}}} \right). \tag{23}$$

The $\mathrm{Ca_V}1.2$ model of Faber et al. [6] is used for the current across L-type Ca^{2+} channels. The voltage-dependent gating mode of the channel is considered, which includes four closed states (c_0, c_1, c_2, and c_3), one open state (p_o), and fast (i_{vf}) and slow (i_{vs}) inactivated states. The corresponding equations are

$$I_{\mathrm{Ca,L}} = G_{\mathrm{CaL}} p_{\mathrm{o}} \left(V_{\mathrm{m}} - E_{\mathrm{Ca}} \right), \tag{24a}$$
$$\frac{dc_0}{dt} = \beta c_1 - (4\alpha) c_0, \tag{24b}$$
$$\frac{dc_1}{dt} = (4\alpha) c_0 + (2\beta) c_2 - (3\alpha + \beta) c_1, \tag{24c}$$
$$\frac{dc_2}{dt} = (3\alpha) c_1 + (3\beta) c_3 - (2\alpha + 2\beta) c_2, \tag{24d}$$
$$\frac{dc_3}{dt} = (2\alpha) c_2 + (4\beta) p_{\mathrm{o}} + \omega_{\mathrm{f}} i_{\mathrm{vf}} + \omega_{\mathrm{s}} i_{\mathrm{vs}} - (\alpha + 3\beta + \gamma_{\mathrm{f}} + \gamma_{\mathrm{s}}) c_3, \tag{24e}$$
$$\frac{dp_{\mathrm{o}}}{dt} = \alpha c_3 + \lambda_{\mathrm{f}} i_{\mathrm{vf}} + \lambda_s i_{\mathrm{vs}} - (4\beta + \phi_{\mathrm{f}} + \phi_{\mathrm{s}}) p_{\mathrm{o}}, \tag{24f}$$
$$\frac{di_{\mathrm{vf}}}{dt} = \gamma_{\mathrm{f}} c_3 + \phi_{\mathrm{f}} p_{\mathrm{o}} + \omega_{\mathrm{sf}} i_{\mathrm{vs}} - (\omega_{\mathrm{f}} + \lambda_{\mathrm{f}} + \omega_{\mathrm{fs}}) i_{\mathrm{vf}}, \tag{24g}$$
$$\frac{di_{\mathrm{vs}}}{dt} = \gamma_{\mathrm{s}} c_3 + \phi_{\mathrm{s}} p_{\mathrm{o}} + \omega_{\mathrm{fs}} i_{\mathrm{vf}} - (\omega_{\mathrm{s}} + \lambda_{\mathrm{s}} + \omega_{\mathrm{sf}}) i_{\mathrm{vs}}, \tag{24h}$$

where

$$\begin{aligned}
\alpha &= 0.925 \exp(V_{\mathrm{m}}/30), & \beta &= 0.390 \exp(V_{\mathrm{m}}/40), \\
\gamma_{\mathrm{f}} &= 0.245 \exp(V_{\mathrm{m}}/10), & \gamma_{\mathrm{s}} &= 0.005 \exp(-V_{\mathrm{m}}/40), \\
\phi_{\mathrm{f}} &= 0.020 \exp(V_{\mathrm{m}}/500), & \phi_{\mathrm{s}} &= 0.030 \exp(-V_{\mathrm{m}}/280), \\
\lambda_{\mathrm{f}} &= 0.035 \exp(-V_{\mathrm{m}}/300), & \lambda_{\mathrm{s}} &= 0.0011 \exp(V_{\mathrm{m}}/500), \\
\omega_{\mathrm{f}} &= (4\beta\lambda_{\mathrm{f}}\gamma_{\mathrm{f}})/(\alpha\phi_{\mathrm{f}}), & \omega_{\mathrm{s}} &= (4\beta\lambda_{\mathrm{s}}\gamma_{\mathrm{s}})/(\alpha\phi_{\mathrm{s}}), \\
\omega_{\mathrm{sf}} &= (\lambda_{\mathrm{s}}\phi_{\mathrm{f}})/\lambda_{\mathrm{f}}, & \omega_{\mathrm{fs}} &= \phi_{\mathrm{s}}.
\end{aligned}$$

T-type Ca^{2+} channels are not considered in the Edwards and Layton [5] model.

The current across sarco/endoplasmic reticulum Ca^{2+} (SERCA) pumps is given by

$$I_{\mathrm{SERCA}} = I_{\mathrm{SERCA,max}} \left(\frac{[\mathrm{Ca}]^2_{\mathrm{cyt}}}{\left(K^{\mathrm{Ca}}_{\mathrm{m,SERCA}}\right)^2 + [\mathrm{Ca}]^2_{\mathrm{cyt}}} \right). \tag{25}$$

The RyR model of Keizer and Levine [10] is used to determine the RyR-mediated release current into the cytosol,

$$I_{\mathrm{RyR}} = v_{\mathrm{RyR}} P_{\mathrm{RyR}} \left([\mathrm{Ca}]_{\mathrm{SR}} - [\mathrm{Ca}]_{\mathrm{cyt}} \right) (2F \cdot \mathrm{vol}_{\mathrm{SR}}), \tag{26}$$

where v_{RyR} is the RyR rate constant. The open probability of RyR (P_{RyR}) is calculated as

$$P_{\mathrm{RyR}} = \frac{\omega\left(1+\left([\mathrm{Ca}]_{\mathrm{cyt}}/K_{\mathrm{b}}\right)^3\right)}{1+\left(K_{\mathrm{a}}/[\mathrm{Ca}]_{\mathrm{cyt}}\right)^4+\left([\mathrm{Ca}]_{\mathrm{cyt}}/K_{\mathrm{b}}\right)^3}, \tag{27a}$$

$$\frac{d\omega}{dt} = \frac{k_{\mathrm{c}}^{-}\left(\omega^{\infty}-\omega\right)}{\omega^{\infty}}, \tag{27b}$$

$$\omega^{\infty} = \frac{1+\left(K_{\mathrm{a}}/[\mathrm{Ca}]_{\mathrm{cyt}}\right)^4+\left([\mathrm{Ca}]_{\mathrm{cyt}}/K_{\mathrm{b}}\right)^3}{1+1/K_{\mathrm{c}}+\left(K_{\mathrm{a}}/[\mathrm{Ca}]_{\mathrm{cyt}}\right)^4+\left([\mathrm{Ca}]_{\mathrm{cyt}}/K_{\mathrm{b}}\right)^3}. \tag{27c}$$

The IP_3R model of De Young and Keizer [2] is used to determined the IP_3R-mediated release current in the cytosol,

$$I_{\mathrm{IP3R}} = v_{\mathrm{IP3R}}(x_{110})^3\left([\mathrm{Ca}]_{\mathrm{SR}}-[\mathrm{Ca}]_{\mathrm{cyt}}\right)(2F\cdot\mathrm{vol}_{\mathrm{SR}}), \tag{28}$$

where v_{IP3R} is the IP_3R rate constant and x_{110} is the fraction of receptors bound by one activated Ca^{2+} and one IP_3, calculated as described below. The cytosolic concentration of IP_3 is calculated as

$$\frac{d[\mathrm{IP_3}]_{\mathrm{cyt}}}{dt} = k_{+}^{\mathrm{IP3}}[\mathrm{IP_3}]_{\mathrm{ref}}\left(\frac{[\mathrm{Ca}]_{\mathrm{cyt}}+(1-\alpha_4)k_4}{[\mathrm{Ca}]_{\mathrm{cyt}}+k_4}\right)-k_{-}^{\mathrm{IP3}}[\mathrm{IP_3}]_{\mathrm{cyt}}, \tag{29}$$

where k_{+}^{IP3} and k_{-}^{IP3} are the rate constants for IP_3 formation and consumption, respectively, $[\mathrm{IP_3}]_{\mathrm{ref}}$ is a reference IP_3 concentration, and α_4 determines the strength of the Ca^{2+} feedback on IP_3 production.

Three equivalent and independent IP_3R subunits are assumed to be involved in conduction, and each subunit has one IP_3 binding site (denoted as *site 1*) and two Ca^{2+} binding sites, one for activation (*site 2*) and one for inhibition (*site 3*). The fraction of receptors in state $S_{i_1i_2i_3}$ is denoted by $x_{i_1i_2i_3}$, where i_j equals 0 if the j-th binding site is unoccupied or 1 if it is occupied. All three subunits must be in the state S_{110} (corresponding to the binding of one IP_3 and one activating Ca^{2+}) for the IP_3R channel to be open. Assuming rapid equilibrium for IP_3 binding,

$$a_1[\mathrm{Ca}]_{\mathrm{cyt}}x_{0k0} = b_1x_{1k0}, \qquad k=0,1, \tag{30a}$$

$$a_3[\mathrm{Ca}]_{\mathrm{cyt}}x_{0k1} = b_3x_{1k1}, \qquad k=0,1. \tag{30b}$$

Defining $d_k = b_k/a_k$, the conservation equations for $x_{0i_2i_3}$ are

$$\frac{dx_{000}}{dt} = -a_4\left([\mathrm{Ca}]_{\mathrm{cyt}}x_{000} - d_4x_{001}\right) - a_5\left([\mathrm{Ca}]_{\mathrm{cyt}}x_{000} - d_5x_{010}\right), \tag{31a}$$

$$\frac{dx_{001}}{dt} = +a_4\left([\mathrm{Ca}]_{\mathrm{cyt}}x_{000} - d_4x_{001}\right) - a_5\left([\mathrm{Ca}]_{\mathrm{cyt}}x_{001} - d_5x_{011}\right), \tag{31b}$$

$$\frac{dx_{010}}{dt} = +a_5\left([\mathrm{Ca}]_{\mathrm{cyt}}x_{000} - d_5x_{010}\right) - a_4\left([\mathrm{Ca}]_{\mathrm{cyt}}x_{010} - d_4x_{011}\right), \tag{31c}$$

$$x_{011} = 1 - (x_{000} + x_{001} + x_{010} + x_{100} + x_{101} + x_{110} + x_{111}). \tag{31d}$$

5.2 Intracellular Ca^{2+} Dynamics

5.2.1 Calcium buffers

Calcium buffering by calmodulin and other Ca^{2+}-binding proteins in the cytosol is described as a first-order dynamic process,

$$\frac{d[\mathrm{Bf}\cdot\mathrm{Ca}]_{\mathrm{cyt}}}{dt} = k_{\mathrm{on}}^{\mathrm{Bf}}[\mathrm{Ca}]_{\mathrm{cyt}}\left([\mathrm{Bf}]_{\mathrm{cyt}}^{\mathrm{tot}} - [\mathrm{Bf}\cdot\mathrm{Ca}]_{\mathrm{cyt}}\right) - k_{\mathrm{off}}^{\mathrm{Bf}}[\mathrm{Bf}\cdot\mathrm{Ca}]_{\mathrm{cyt}}, \tag{32}$$

where $[\mathrm{Bf}]_{\mathrm{cyt}}^{\mathrm{tot}}$ is the total concentration of Ca^{2+}-binding proteins other than calmodulin in the cytosol and $[\mathrm{Bf}\cdot\mathrm{Ca}]_{\mathrm{cyt}}$ is the concentration of the calcium-bound sites of these other buffering elements.

Calcium buffering by calsequestrin in the SR is described as

$$\frac{d[\mathrm{Calseq}\cdot\mathrm{Ca}]_{\mathrm{SR}}}{dt} = k_{\mathrm{on}}^{\mathrm{Calseq}}[\mathrm{Ca}]_{\mathrm{SR}}\left([\mathrm{Calseq}]_{\mathrm{SR}}^{\mathrm{tot}} - [\mathrm{Calseq}\cdot\mathrm{Ca}]_{\mathrm{SR}}\right) - k_{\mathrm{off}}^{\mathrm{Calseq}}[\mathrm{Calseq}\cdot\mathrm{Ca}]_{\mathrm{SR}}, \tag{33}$$

where $[\mathrm{Calseq}]_{\mathrm{SR}}^{\mathrm{tot}}$ is the total concentration of calsequestrin sites available for Ca^{2+} binding in the SR and $[\mathrm{Calseq}\cdot\mathrm{Ca}]_{\mathrm{SR}}$ is the concentration of Ca^{2+}-bound calsequestrin sites in that compartment. Parameter values are given in Table 6.

5.3 Kinetics of Myosin Light Chain Phosphorylation

5.3.1 CaM activation of MLCK

Calmodulin (CaM) has four Ca^{2+} binding sites, with two at the NH_2 terminus (low affinity) and two at the COOH terminus (high affinity). Binding of Ca^{2+} to those sites yields the $CaM.Ca_4$ complex, and $CaM.Ca_4$ binds to myosin light chain kinase (MLCK) to form $MLCK.CaM.Ca_4$, which is the active form of MLCK that phosphorylates MLCs.

The scheme proposed by Fajmut et al. [7] is used to determine the kinetics of formation of MLCK.CaM.Ca_4. Subscripts N and C represent two binding sites each for Ca^{2+} at the NH_2 and COOH terminus of CaM, respectively, and the subscript M represents the CaM binding site occupied by MLCK. An underscore (_) denotes an unoccupied site for each of these binding sites. For example, CaM_{NCM} designates MLCK.CaM.Ca_4. The kinetic equations for the formation of MLCK are

$$\begin{aligned}\frac{d[\mathrm{CaM_{-C-}}]}{dt} &= \left(-k_{-1}^{\mathrm{CaM}} - k_4^{\mathrm{CaM}}[\mathrm{Ca}]^2 - k_5^{\mathrm{CaM}}[\mathrm{MLCK}]_{\mathrm{free}}\right)[\mathrm{CaM_{-C-}}] \\ &\quad + k_1^{\mathrm{CaM}}[\mathrm{Ca}]^2[\mathrm{CaM_{---}}] + k_{-4}^{\mathrm{CaM}}[\mathrm{CaM_{NC-}}] + k_{-5}^{\mathrm{CaM}}[\mathrm{CaM_{-CM}}], \end{aligned} \tag{34a}$$

$$\begin{aligned}\frac{d[\mathrm{CaM_{N--}}]}{dt} &= \left(-k_{-2}^{\mathrm{CaM}} - k_3^{\mathrm{CaM}}[\mathrm{Ca}]^2\right)[\mathrm{CaM_{N--}}] + k_2^{\mathrm{CaM}}[\mathrm{Ca}]^2[\mathrm{CaM_{---}}] \\ &\quad + k_{-3}^{\mathrm{CaM}}[\mathrm{CaM_{NC-}}], \end{aligned} \tag{34b}$$

$$\begin{aligned}\frac{d[\mathrm{CaM_{NC-}}]}{dt} &= \left(-k_{-3}^{\mathrm{CaM}} - k_{-4}^{\mathrm{CaM}} - k_7^{\mathrm{CaM}}[\mathrm{MLCK}]_{\mathrm{free}}\right)[\mathrm{CaM_{NC-}}] \\ &\quad + k_3^{\mathrm{CaM}}[\mathrm{Ca}]^2[\mathrm{CaM_{N--}}] + k_4^{\mathrm{CaM}}[\mathrm{Ca}]^2[\mathrm{CaM_{-C-}}] \\ &\quad + k_{-7}^{\mathrm{CaM}}[\mathrm{Ca}]^2[\mathrm{CaM_{NCM}}], \end{aligned} \tag{34c}$$

$$\begin{aligned}\frac{d[\mathrm{CaM_{-CM}}]}{dt} &= \left(-k_{-5}^{\mathrm{CaM}} - k_6^{\mathrm{CaM}}[\mathrm{Ca}]^2\right)[\mathrm{CaM_{-CM}}] + k_5^{\mathrm{CaM}}[\mathrm{MLCK}]_{\mathrm{free}}[\mathrm{CaM_{-C-}}] \\ &\quad + k_{-6}^{\mathrm{CaM}}[\mathrm{Ca}]^2[\mathrm{CaM_{NCM}}], \end{aligned} \tag{34d}$$

$$\begin{aligned}\frac{d[\mathrm{CaM_{NCM}}]}{dt} &= \left(-k_{-6}^{\mathrm{CaM}} - k_{-7}^{\mathrm{CaM}}[\mathrm{Ca}]^2\right)[\mathrm{CaM_{NCM}}] + k_6^{\mathrm{CaM}}[\mathrm{Ca}]^2[\mathrm{CaM_{-CM}}] \\ &\quad + k_7^{\mathrm{CaM}}[\mathrm{MLCK}]_{\mathrm{free}}[\mathrm{CaM_{NC-}}], \end{aligned} \tag{34e}$$

$$\begin{aligned}[\mathrm{CaM}]^{\mathrm{tot}} &= [\mathrm{CaM_{---}}] + [\mathrm{CaM_{-C-}}] + [\mathrm{CaM_{N--}}] + [\mathrm{CaM_{NC-}}], \\ &\quad + [\mathrm{CaM_{-CM}}] + [\mathrm{CaM_{NCM}}], \end{aligned} \tag{34f}$$

$$[\mathrm{MLCK}]^{\mathrm{tot}} = [\mathrm{CaM_{-CM}}] + [\mathrm{CaM_{NCM}}] + [\mathrm{MLCK}]_{\mathrm{free}}, \tag{34g}$$

where the on- and off-rate constants are denoted by k_i^{CaM} and k_{-i}^{CaM}, respectively, $[\mathrm{MLCK}]_{\mathrm{free}}$ is the concentration of free (unbound) MLCK, $[\mathrm{CaM}]^{\mathrm{tot}}$ is the total concentration of calmodulin, $[\mathrm{MLCK}]^{\mathrm{tot}}$ is the total concentration of MLCK, and the subscript "cyt" that denotes the cytosolic compartment is omitted for simplicity. Parameter values are given in Table 7.

The buffering terms in the Ca^{2+} conservation equations (12d) and (13) are given by

$$R_{\mathrm{CaM}}^{\mathrm{cyt}} = -2\frac{d[\mathrm{CaM_{N--}}]}{dt} - 2\frac{d[\mathrm{CaM_{-C-}}]}{dt} - 2\frac{d[\mathrm{CaM_{-CM}}]}{dt} - 4\frac{d[\mathrm{CaM_{NC-}}]}{dt} - 4\frac{d[\mathrm{CaM_{NCM}}]}{dt}, \tag{35a}$$

$$R_{\mathrm{Bf}}^{\mathrm{cyt}} = -\frac{d[\mathrm{Bf}\cdot\mathrm{Ca}]_{\mathrm{cyt}}}{dt}, \tag{35b}$$

$$R_{\mathrm{Calseq}}^{\mathrm{SR}} = -\frac{d[\mathrm{Calseq}\cdot\mathrm{Ca}]_{\mathrm{SR}}}{dt}. \tag{35c}$$

5.3.2 Rho-kinase inhibition of MLCP

Myosin light chain phosphatase (MLCP) consists of three subunits, one of which, MYPT1, can be phosphorylated by Rho kinase (RhoK). Rho-K-induced phosphorylation of MYPT1 inactivates MLCP, which promotes contraction. The cytosolic concentration of active MLCP (denoted MLCP*) is given by

$$\frac{d[\mathrm{MLCP}^*]}{dt} = k_+^{\mathrm{MLCP}}\left([\mathrm{MLCP}]^{\mathrm{tot}} - [\mathrm{MLCP}^*]\right) - k_-^{\mathrm{MLCP}}[\mathrm{MLCP}^*], \tag{36}$$

where $[\mathrm{MLCP}]^{\mathrm{tot}}$ is the total concentration of MLCP in the cytosol and the inactivation of MLCP by RHoK is given by

$$k_-^{\mathrm{MLCP}} = k_{\mathrm{cat}}[\mathrm{RhoK}] \tag{37}$$

(Mbikou et al. [13]). The concentration of RhoK, $[\mathrm{RhoK}]$, is assumed to be fixed at 30 nM (Kaneko-Kawano et al. [9]) except in the presence of specific inhibitors. Parameter values are given in Table 7.

Table 7 Parameters for MLCK and MLCP kinetics

Parameter	Value	Unit
k_1^{CaM}	2.8×10^6	$\mathrm{mM}^{-1}\cdot\mathrm{s}^{-1}$
k_{-1}^{CaM}	6	s^{-1}
k_2^{CaM}	10^8	$\mathrm{mM}^{-1}\cdot\mathrm{s}^{-1}$
k_{-2}^{CaM}	800	s^{-1}
k_3^{CaM}	2.8×10^6	$\mathrm{mM}^{-1}\cdot\mathrm{s}^{-1}$
k_{-3}^{CaM}	6	s^{-1}
k_4^{CaM}	10^8	$\mathrm{mM}^{-1}\cdot\mathrm{s}^{-1}$
k_{-4}^{CaM}	800	s^{-1}
k_5^{CaM}	10^9	$\mathrm{mM}^{-1}\cdot\mathrm{s}^{-1}$
k_{-5}^{CaM}	20	s^{-1}
k_6^{CaM}	1.25×10^7	$\mathrm{mM}^{-1}\cdot\mathrm{s}^{-1}$
k_{-6}^{CaM}	5	s^{-1}
k_7^{CaM}	10^9	$\mathrm{mM}^{-1}\cdot\mathrm{s}^{-1}$

Parameter	Value	Unit
k_{-7}^{CaM}	1	s^{-1}
$[\mathrm{CaM}]^{\mathrm{tot}}$	10×10^{-3}	mM
$[\mathrm{MLCK}]^{\mathrm{tot}}$	2×10^{-3}	mM
$[\mathrm{MLCP}]^{\mathrm{tot}}$	2×10^{-3}	mM
$[\mathrm{RhoK}]$	30×10^{-6}	mM
$k_{\mathrm{cat}}/k_+^{\mathrm{MLCP}}$	0.33×10^6	mM^{-1}
$k_{\mathrm{MLCK}}^{\mathrm{Myo}}$	0.537	s^{-1}
$k_{\mathrm{MLCP}}^{\mathrm{Myo}}$	1.62	s^{-1}
k_3^{Myo}	1.8	s^{-1}
k_4^{Myo}	0.1	s^{-1}
k_7^{Myo}	0.045	s^{-1}
$[\mathrm{Myo}]^{\mathrm{tot}}$	30×10^{-3}	mM

5.3.3 MLCK- and MLCP-dependent phosphorylation of myosin

The contractile force of the vessels is determined by the fraction of myosin cross-bridges that are phosphorylated. The four types of cross-bridges considered are free cross-bridges (Myo), phosphorylated cross-bridges (MyoP), attached phosphorylated cycling cross-bridges (AMyoP), and attached dephosphorylated, non-cycling cross-bridges (AMyo), and the corresponding equations for their concentrations are

$$\frac{d[\mathrm{Myo}]}{dt} = -k_1^{\mathrm{Myo}}[\mathrm{Myo}] + k_2^{\mathrm{Myo}}[\mathrm{MyoP}] + k_7^{\mathrm{Myo}}[\mathrm{AMyo}], \tag{38a}$$

$$\frac{d[\mathrm{MyoP}]}{dt} = +k_1^{\mathrm{Myo}}[\mathrm{Myo}] - (k_2^{\mathrm{Myo}} + k_3^{\mathrm{Myo}})[\mathrm{MyoP}] + k_4^{\mathrm{Myo}}[\mathrm{AMyoP}], \tag{38b}$$

$$\frac{d[\mathrm{AMyoP}]}{dt} = +k_3^{\mathrm{Myo}}[\mathrm{MyoP}] - (k_4^{\mathrm{Myo}} + k_5^{\mathrm{Myo}})[\mathrm{AMyoP}] + k_6^{\mathrm{Myo}}[\mathrm{AMyo}], \tag{38c}$$

$$[\mathrm{Myo}]^{\mathrm{tot}} = [\mathrm{Myo}] + [\mathrm{MyoP}] + [\mathrm{AMyoP}] + [\mathrm{AMyo}]. \tag{38d}$$

The rate constants k_3^{Myo}, k_4^{Myo}, and k_7^{Myo} are fixed (Yang et al. [19]). Parameter values are given in Table 7.

The rate constants k_1^{Myo} and k_6^{Myo} represent the activity of MLCK and are assumed to be proportional to the fraction of the fully activated form of the enzyme, while the rate constants k_2^{Myo} and k_5^{Myo} represent the activity of MLCP. The corresponding equations are

$$k_1^{\mathrm{Myo}} = k_6^{\mathrm{Myo}} = k_{\mathrm{MLCK}}^{\mathrm{Myo}} \frac{[\mathrm{CaM_{NCM}}]}{[\mathrm{CaM}]^{\mathrm{tot}}}, \tag{39a}$$

$$k_2^{\mathrm{Myo}} = k_5^{\mathrm{Myo}} = k_{\mathrm{MLCP}}^{\mathrm{Myo}} \frac{[\mathrm{MLCP}^*]}{[\mathrm{MLCP}]^{\mathrm{tot}}}, \tag{39b}$$

where $k_{\mathrm{MLCK}}^{\mathrm{Myo}}$ and $k_{\mathrm{MLCP}}^{\mathrm{Myo}}$ are fixed.

5.4 Mechanical Behavior of Cell

The vasomotion of the afferent arteriole is affected by the variations in the number of crossbridges, which induce variations in the contractile force and thus alter the diameter of the vessel. Edwards and Layton [5] implemented the model of Carlson et al. [1] that represents vessel wall tension as the sum of a passive component and an active myogenic component. The passive component, T_{pass}, is a function of the vessel diameter, D,

$$T_{\mathrm{pass}} = C_{\mathrm{pass}} \exp\left[C'_{\mathrm{pass}}\left(\frac{D}{D_0} - 1\right)\right], \tag{40}$$

where D_0 is the reference vessel diameter.

The active myogenic component is the product of the maximal active tension generated at a given vessel circumference, $T_{\text{act}}^{\max}$, given by

$$T_{\text{act}}^{\max} = C_{\text{act}} \exp\left[-\left(\frac{D/D_0 - C'_{\text{act}}}{C''_{\text{act}}}\right)^2\right], \tag{41}$$

and the fraction of myosin light chains that are phosphorylated, Ψ. Therefore the total tension in the wall, T_{wall}, is

$$T_{\text{wall}} = T_{\text{pass}} + \Psi T_{\text{act}}^{\max}. \tag{42}$$

The change in vessel diameter depends on the difference between the tension resulting from intravascular pressure p, $T_{\text{pres}} = pD/2$, and the tension generated in the wall, T_{wall}, so that

$$\frac{dD}{dt} = \frac{1}{\tau_{\text{d}}} \frac{D_{\text{c}}}{T_{\text{c}}} (T_{\text{pres}} - T_{\text{wall}}), \tag{43}$$

where D_{c} is a reference diameter, T_{c} is the tension at a pressure of 100 mmHg and diameter D_{c}, and τ_{d} is a time constant. Parameter values are given in Table 8.

Table 8 Parameters for smooth muscle cell mechanics

Parameter	Value	Unit
C_{pass}	223	dyn/cm
C'_{pass}	20.2	dimensionless
C_{act}	500	dyn/cm
C'_{act}	0.985	dimensionless
C''_{act}	0.500	dimensionless
D_0	27.5	μm
D_{c}	20.0	μm
τ_{d}	1.71	s

Acknowledgements

This work is the product of a workshop and short-term visits supported by the National Institute for Mathematical and Biological Synthesis, an Institute sponsored by the National Science Foundation through NSF Award #DBI-1300426, with additional support from The University of Tennessee, Knoxville. Support was also provided by the National Institutes of Health: National Institute of Diabetes and Digestive and Kidney Diseases and by the National Science Foundation, via grants #DK089066 and #DMS-1263995 to AT Layton.

References

1. Carlson, B.E., Arciero, J.C., Secomb, T.W.: Theoretical model of blood flow autoregulation: roles of myogenic, shear-dependent, and metabolic responses. Am J Physiol Heart Circ Physiol **295**, H1572–H1579 (2008)
2. De Young, G.W., Keizer, J.: A single-pool inositol 1,4,5-triphosphate-receptor-based model for agonist-stimulated oscillations in Ca^{2+} concentrations. Proc Natl Acad Sci USA **89**, 9895–9899 (1992)
3. Deen, W., Robertson, C., Brenner, B.: A model of glomerular ultrafiltration in the rat. Am J Physiol **223**(5), 1178–1183 (1972)
4. Eaton, D., Pooler, J.: Vander's Renal Physiology, 6th edn. McGraw-Hill Medical, New York (2004)
5. Edwards, A., Layton, A.: Calcium dynamics underlying the afferent arteriole myogenic response. Am J Physiol Renal Physiol **306**, F34–F48 (2014)
6. Faber, G.M., Silva, J., Livshitz, L., Rudy, Y.: Kinetic properties of the cardiac L-type Ca^{2+} channel and its role in myocyte electrophysiology: a theoretical investigation. Biophys J **92**, 1522–1543 (2007)
7. Fajmut, A., Jagodič, M., Brumen, M.: Mathematical modeling of the myosin light chain kinase activation. Chem Inf Model **45**, 1605–1609 (2005)
8. Jacobsen, J.C.B., Aalkjær, C., Nilsson, H., Matchkov, V.V., Freiberg, J., Holstein-Rathlou, N.H.: Activation of a cGMP-sensitive calcium-dependent chloride channel may cause transition from calcium waves to whole cell oscillations in smooth muscle cells. Am J Physiol Heart Circ Physiol **293**, H215–H228 (2007)
9. Kaneko-Kawano, T., Takasu, F., Naoki, H., Sakumura, Y., Ishii, S., Ueba, T., Eiyama, A., Okada, A., Kawano, Y., Suzuki, K.: Dynamic regulation of myosin light chain phosphorylation by Rho-kinase. PLoS One **7**, e39,269 (2012)
10. Keizer, J., Levine, L.: Ryanodine receptor adaptation and Ca^{2+}-induced Ca^{2+} release dependent Ca^{2+} oscillations. Biophys J **71**, 3477–3487 (1996)
11. Kneller, J., Ramirez, R.J., Chartier, D., Courtemanche, M., Nattel, S.: Time-dependent transients in an ionically based mathematical model of the canine atrial action potential. Am J Physiol Heart Circ Physiol **282**, H1437–H1451 (2002)
12. Layton, A.: Feedback-mediated dynamics in a model of a compliant thick ascending limb. Math Biosci **228**, 185–194 (2010)
13. Mbikou, P., Fajmut, A., Brumen, M., Roux, E.: Contribution of Rho kinase to the early phase of the calcium-contraction coupling in airway smooth muscle. Exp Physiol **96**, 240–258 (2011)
14. Schnermann, J., Briggs, J.: Function of the juxtaglomerular apparatus: Control of glomerular hemodynamics and renin secretion. In: A. RJ, H. SC (eds.) Seldin and Giebisch's The Kidney: Physiology and Pathophysiology, 4th edn., pp. 589–626. Elsevier Academic Press, Amsterdam; Boston (2008)
15. Sgouralis, I., Layton, A.: Autoregulation and conduction of vasomotor responses in a mathematical model of the rat afferent arteriole. Am J Physiol Renal Physiol **303**, F229–F239 (2012)
16. Sgouralis, I., Layton, A.: Theoretical assessment of renal autoregulatory mechanisms. Am J Physiol Renal Physiol **306**, F1357–F1371 (2014)
17. Shannon, T.R., Wang, F., Puglisi, J., Weber, C., Bers, D.M.: A mathematical treatment of integrated Ca dynamics within the ventricular myocyte. Biophys J **87**, 3351–3371 (2004)
18. Wu, B.N., Luykenaar, K.D., Brayden, J.E., Giles, W.R., Corteling, R.L., Wiehler, W.B., Welsh, D.G.: Hyposmotic challenge inhibits inward rectifying K^+ channels in cerebral arterial smooth muscle cells. Am J Physiol Heart Circ Physiol **292**, H1085–H1094 (2007)
19. Yang, J., Clark Jr., J.W., Bryan, R.M., Robertson, C.: The myogenic response in isolated rat cerebrovascular arteries: smooth muscle cell model. Med Eng Phys **25**, 691–709 (2003)